the volume of ^{36}A is 0.2% larger than that of ^{40}A. The results are shown in Figs. 1–3, with experimental data of Batchelder *et al.*,[14] and Egger *et al.*[15] The measurements of Egger *et al.* were made with natural argon and the frequencies have been increased by the factor $(\frac{40}{36})^{1/2}$.

The agreement with experiment is very good, considerably better than was found with nearest-neighbor 6-12 and 6-13 interactions by Goldman *et al.*,[2] and also considerably better than was found with five-parameter second-nearest-neighbor models by Batchelder *et al.*[14] This is particularly noticeable for the longitudinal ⟨110⟩ waves, for which none of the other models is satisfactory.

It is to be noticed that the unconstrained five-parameter fit of Batchelder *et al.* gave elastic constants (in units of 10^{10} dyn cm^{-2}) $c_{11}=4.11$, $c_{12}=1.90$, $c_{44}=2.10$, and $A=1.9$. These are appreciably closer to our theoretical values ($c_{11}=4.16$, $c_{12}=2.30$, $c_{44}=2.28$; $A=2.5$) than are the ultrasonic results of Keeler and Batchelder[8] ($c_{11}=4.39$, $c_{12}=1.83$, $c_{44}=1.64$; $A=1.28$), particularly in the value of c_{44}. The value of A is also much closer to all theoretical estimates.

ACKNOWLEDGMENT

We are grateful to Dr. T. R. Koehler for assistance in checking the reliability of our approximate method for calculating anharmonic frequency shifts.

*Permanent address: National Research Council, Ottawa, Canada.

[1]C. Feldman, M. L. Klein, and G. K. Horton, Phys. Rev. 184, 910 (1969).

[2]V. V. Goldman, G. K. Horton, T. H. Keil, and M. L. Klein, J. Phys. C 3, L33 (1970).

[3]M. V. Bobetic and J. A. Barker, preceding paper, Phys. Rev. B 2, 4169 (1970).

[4]G. G. Chell and I. J. Zucker, J. Phys. C 1, 35 (1968); I. J. Zucker and G. G. Chell, *ibid.* 1, 1505 (1968).

[5]W. Goetze and H. Schmidt, Z. Physik 192, 409 (1966).

[6]A. Huller, W. Goetze, and H. Schmidt, Z. Physik 231, 173 (1970).

[7]T. H. K. Barron and M. L. Klein, Proc. Phys. Soc. (London) 85, 533 (1965).

[8]G. J. Keeler and D. N. Batchelder, J. Phys. C 3, 510 (1970).

[9]J. De Launay, J. Chem. Phys. 22, 1676 (1954).

[10]J. A. Barker, M. L. Klein, and M. V. Bobetic (unpublished).

[11]O. G. Peterson, D. N. Batchelder, and R. O. Simmons, Phys. Rev. 150, 703 (1966).

[12]J. W. Stewart, Phys. Rev. 97, 578 (1955).

[13]W. G. Hoover, A. C. Holt, and D. R. Squire, Physica 44, 437 (1969).

[14]D. N. Batchelder, M. F. Collins, B. C. G. Haywood, and G. R. Sidey, J. Phys. C 3, 249 (1970).

[15]H. A. Egger, M. Gsanger, E. Luscher, and B. Dorner, Phys. Letters 28A, 433 (1968).

PHYSICAL REVIEW B VOLUME 2, NUMBER 10 15 NOVEMBER 1970

Vibronic Aspects of the CaO and MgO *F* Bands*†

Bruce D. Evans and James C. Kemp
Department of Physics, University of Oregon, Eugene, Oregon 97403
(Received 4 June 1970)

A useful extension is made to the existing theory of the optical absorption and emission bands of defects and impurities in low concentrations in crystalline host materials. This extension is able to account for the shape of the low-temperature absorption and emission bands in both the details of the sharp-line phonon-related peaks and the broad-band characteristics—as applications to defect centers in the alkaline-earth oxides (and alkali halides) demonstrate. A lifetime-broadening mechanism is introduced to explain the observed smearing and broadening of higher-energy multiple-phonon-assisted transitions, the manifold of such transitions giving rise to the broad band. We then specialize to the case of *F* centers in cubic (O_h group) materials; a short group-theoretical discussion shows for this case that only local modes belonging to the Γ_1^+, Γ_{12}^+, and Γ_{25}^+ representations may be active and that both transverse and longitudinal acoustic lattice modes near the *L* band point are expected to be most active in coupling the single trapped electron to the lattice. Comparison is made with recent experimental results for the *F* center in CaO and MgO.

INTRODUCTION

Many impurity and defect centers in solids show Gaussian absorption and emission bands.[1] Partly as a result of this and partly for the sake of mathematical convenience most optical theories of these centers assume *a priori* these bands to be Gaussian or very nearly so.[2] We present below in Sec. I a simple extension of these optical theories by carrying out explicitly the sum over inner products of

the vibrational part of the total vibronic dipole matrix element, i.e., a sum of Frank-Condon overlaps. Considering local vibrational modes, simple well-known harmonic oscillator functions are used for these vibrational wave functions. For many cases of interest the sum has less than twenty terms, allowing the use of a short computer program and a plotted output. We introduce a lifetime-broadening mechanism to account for the observed broadening and smearing of individual higher-energy vibronic transitions for defect centers in the alkaline-earth oxides and alkali halides. The broadening mechanism is essentially derived from the time-dependent first-order perturbation of the zero-point host lattice motion upon the local-mode eigenvectors. The results of Sec. I are general enough to have applications to the understanding of optical spectra of many molecular systems.

Section II applies the results of group theory to the special case of the F-center defect in cubic materials to determine which perfect-lattice modes and which local modes (involving only the six nearest-neighbor ions) may actively assist the electronic transition from the ground to the first excited state. Since much of the necessary group-theoretical formalism for this problem has been carried out by others, we merely present the results. Special attention is now paid to the CaO lattice as the F center in this case proves to have one of the more spectroscopically interesting vibronic structure in its absorption and emission bands.

Section III compares the results of Sec. I with our recent observed absorption and emission bands for the F center in CaO and MgO, which represent, respectively, two extreme cases of small and large electron-lattice coupling parameters (Huang-Rhys factors). Also an illustrative example is made of the R_2 absorption band in LiF.

I. THEORY

The induced absorption coefficient in the dipole approximation is usually written as[3]

$$\alpha(\omega) = (N_0 4\pi^2\omega/3\hbar c)\left|\vec{\mu}\right|^2, \tag{1}$$

where the dipole matrix element

$$\vec{\mu} = \int \Psi_{\text{final}}(\vec{r}) e\vec{r}\, \Psi_{\text{initial}}(\vec{r})\, d\vec{r}$$

and N_0 is the density of absorbing elements (atoms, ions, molecules, defect centers, impurities, etc.). Also, the intensity of radiation due to spontaneous emission is usually written

$$I^e(\omega) = N\hbar\omega A, \tag{2}$$

where N is here the number of centers in the excited level, $\hbar\omega$ the energy released in the transition, and A the Einstein A coefficient for spontaneous emission[1,4]:

$$A = 4\omega^3\left|\vec{\mu}\right|^2/3c^3\hbar. \tag{3}$$

For many impurity and defect centers there are basically two extreme points of view one may take regarding "the system" when considering the system wave functions Ψ_{final} and Ψ_{initial} appearing in the dipole matrix element. Because of the long-range nature of the Coulomb interaction of the trapped electron (or impurity ion, etc.) with the host crystal ions, this electron (impurity ion) really interacts with all the ions of the crystal and may respond to many of the allowed motions (phonons) these ions undergo. Here one would write $\Psi_{\text{system}} = \Psi(r, \theta, \phi, q_1, q_2, \ldots, q_{3N})$, where r, θ, ϕ are coordinates for the trapped electron and q_n runs over the $3N$ coordinates for the N ions in the crystal.

The other extreme viewpoint takes "the system" to be the trapped electron and only its six nearest-neighbor (nn) ions. Further it is assumed that the motions of the six nn ions may be effectively described by a single coordinate q (dominate breathing-mode model). Here $\Psi_{\text{system}} = \Psi(r, \theta, \phi, q)$. It is the purpose of this paper to attempt a marriage of these two points of view in order to better describe the observed optical absorption and emission properties of defect centers, principally the F center in CaO.

The usual application of the Born-Oppenheimer (adiabatic) and Condon approximations[5] allows the integration of the electronic and nuclear parts in the matrix element to proceed separately

$$\Psi_n^{(i)}(\vec{r}, \vec{q}) = \phi_{\vec{q}}^{(i)}(\vec{r})\chi_n^{(i)}(\vec{q}) \simeq \phi_{\langle\vec{q}\rangle}^{(i)}(\vec{r})\chi_n^{(i)}(\vec{q})$$

for the ith electronic state and nth vibration level. Here $\vec{q}$ symbolically represents as many nuclear coordinates as may be practical and necessary to adequately describe the system.

At any nonzero temperature one must average over all the occupied initial vibrational states (m) and sum over all possible final vibrational states (n). Therefore, the matrix element appears as

$$\left|\vec{\mu}(E)\right|^2 = \left|\langle \phi^{(2)}\left|e\vec{r}\right|\phi^{(1)}\rangle\right|^2 \sum_{m=0}^{\infty} p_m(T) \times \sum_{n=0}^{\infty} \left|\langle \chi_n^{(2)}\left|\chi_m^{(1)}\right\rangle\right|^2 \delta(E-(E_f-E_i)),$$

where the δ function is essentially a statement of the Bohr frequency condition and

$$p_m(T) = e^{-\beta\hbar\omega m}(1 - e^{-\beta\hbar\omega}), \quad \beta^{-1} = kT.$$

As exhaustive studies of the electronic wave functions are to be found in the literature,[6,7] we will focus attention on the nuclear part of $\left|\vec{\mu}\right|^2$ from which an interesting energy dependence emerges.

The method by which the nuclear wave functions are handled often depends upon the specific experimental case at hand. For the cases encountered here we find it convenient to first consider the effect of local vibrational modes and later to include (if necessary) the effect of bulk modes due

to the host lattice.

The simplest local-mode approximation is to consider only the six nn cations. The motion of these ions will be harmonic for small displacements about an equilibrium position $[\langle\vec{q}\rangle^{(i)}]$. A description is most easily accomplished in terms of the L normal modes and the L normal coordinates (q_j). Then our initial and final nuclear wave functions for the absorption case will appear as products:

$$\chi_m^{(1)}(\vec{q}) = \prod_{k=1}^{L} \chi_{m_k}^{(1)}(q_k),$$

$$\chi_n^{(2)}(\vec{q}) = \prod_{k=1}^{L} \chi_{n_k}^{(2)}(q_k - \Delta q_k),$$

where the Δq_k describes the local lattice relaxation in mode k to accomodate the excited-state electronic wave function $\phi^{(2)}$. Then we have

$$|\vec{\mu}(E)|^2 \propto \sum_{m_k=0}^{\infty} p_{m_k} \sum_{n_k=0}^{\infty} \prod_{k=1}^{L} |\langle \chi_{n_k}^{(2)}(q_k - \Delta q_k) | \chi_{m_k}^{(1)}(q_k)\rangle|^2 \times \delta[E - (E_{n_k} - E_{m_k})].$$

The nuclear wave functions χ are harmonic-oscillation functions

$$\chi_{n_k}^{(i)}(q_k) = \frac{(m\omega_k^{(i)}/\hbar\pi)^{1/4}}{2^{n_k/2}(n_k!)^{1/2}} e^{-\xi^2/2} H_{n_k}(\xi_k),$$

where $\xi_k^2 = (m\omega_k^{(i)}/\hbar)q_k^2$ and $H_{n_k}(\xi_k)$ are Hermite polynomials.

The general term

$$\langle \chi_{n_k}^{(2)}(q_k - \Delta q_k) | \chi_{m_k}^{(1)}(q_k)\rangle$$

is difficult and not absolutely necessary. Our cases of interest will be at low temperature $[kT \ll \hbar\omega_k^{(i)}]$ where only the lowest initial-state vibrational level is occupied. Hence $m_k \to 0$ for all modes k. We further assume (for mathematical convenience) that, for a given vibrational mode k, the frequency $\omega_k^{(i)}$ will be the same for both electronic states, i.e., $\omega_k^{(1)} = \omega_k^{(2)} \equiv \omega_k$. Often these two frequencies may differ by as much as 25%. In these cases, at higher temperatures, an electronic transition involving a local phonon may be strongly broadened. As we are concerned only with the low-temperature case, this broadening mechanism will not be present and the above assumption of frequency equality will not limit the treatment.

Then the general term appears as

$$|\langle \chi_{n_k}^{(2)}(q_k - \Delta q_k) | \nu_{0_k}^{(1)}(q_k)\rangle|^2 = \frac{(S_k)^{n_k}}{(n_k)!} e^{-S_k},$$

where the Huang-Rhys factor $S_k = m\omega_k(\Delta q_k)^2/2\hbar$. Let

$$B_{k,n_k} = (S_k)^{n_k}/(n_k)!.$$

Then

$$|\vec{\mu}(E)|^2 \propto \sum_{n_k=0}^{\infty} \prod_{k=1}^{L} B_{k,n_k} e^{-S_k} \delta(E - E_0 - E_{\text{vib}}), \qquad (4)$$

where

$$E_{\text{vib}} = \sum_{k=1}^{L} \hbar\omega_k(\tfrac{1}{2} + n_k).$$

Here, in the Bohr frequency condition, we have separated out the electronic (E_0) and vibrational (E_{vib}) energy contributions.

The δ functions yield a series of infinitely sharp lines spaced $\hbar\omega$ apart. One does not *a priori* expect these transitions to be infinitely sharp in energy, nor are they observed as such (see Sec. III B). Therefore, we replace each δ function with a normalized distribution of finite width. A Gaussian distribution is chosen for convenience, although more detailed experimental (and theoretical) work may indicate some other distribution, e.g., Lorentzian, etc.:

$$\delta(E - E_0 - E_{\text{vib}}) \to 1/\sigma_k\sqrt{2\pi} \times \exp\{-[(E - E_0 - E_{\text{vib}})^2/2\sigma_k^2]\}. \qquad (5)$$

We now discuss a broadening mechanism accounting for all or at least part of the finite width observed for each of the n_k transitions. (See Fig. 1.) To this end it is convenient to consider the local (defect) oscillator coupled to an oscillator (or set of oscillators) representing some of the normal modes of vibration of ions in the host crystal. We consider all oscillators as treated quantum mechanically, i.e., with discrete or quasidiscrete energy levels. The local oscillator consists of six nn cations electrostatically bound and centered on the

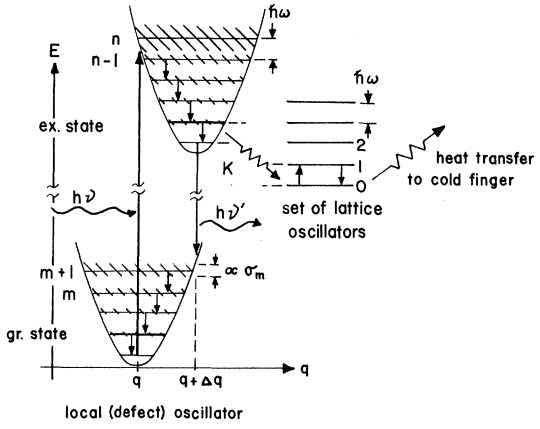

FIG. 1. Width σ_m of each mth local harmonic level is broadened by coupling (K) of the local oscillator to lattice oscillators of the same frequency (ω). That is, the local oscillator transfers (couples) energy into a large set of lattice oscillators which is part of the semi-infinite $(\sim 10^{23})$ ensemble of lattice oscillators, all of which are assumed in a zero-point energy level at low temperatures: $m_{\text{loc}} \to (m-1)_{\text{loc}}$ and 0_{lat}. The density of lattice oscillators in other than the zeroth level is very small so that the probability of the inverse process $[m_{\text{loc}} \to (m+1)_{\text{loc}}$ and $j_{\text{lat}} \to (j-1)_{\text{lat}}]$ is vanishingly small. For convenience only coupling of the excited electronic state is shown.

faces of a cube whose center lies at the anion vacancy. The set of oscillators of varying frequency representing the bulk modes of the host crystal is a mathematical artifice but does, in fact, represent quite well for our purposes the quasicontinuous range of frequencies allowed in the host crystal. More details of the distributions of these lattice frequencies and the nature of the different modes will be discussed later (Sec. II). They are not important for the present argument.

At low temperatures nearly all of the bulk mode oscillators are in their ground states and the initial vibrational state for each mode k is also in its zero-point level as assumed above ($m_k \to 0$). However, after (an assumed Frank-Condon) electronic transition $\phi^{(1)} \to \phi^{(2)}$ the local oscillators of mode k may occupy a number of higher vibrational levels n_k. The center (trapped electron and six nn cations) then "cools off" by emitting phonons into the semi-infinite "cold" reservoir of the bulk crystal. This phonon emission may be considered a degenerate energy transfer between the two oscillators, local and bulk.

The first-order coupling will be a linear term of the form KqQ, where q represents the local oscillator coordinate and Q the bulk oscillator coordinate. K is some "effective" coupling constant whose absolute value in any specific case has little or no physical significance because of the nature of our simplifying assumptions.

Because of the finite lifetime of the local oscillator in excited state n_k, that state will be broadened due to the uncertainty principle $\Delta E \Delta t \sim \hbar$. The lifetime in level n_k is inversely proportional to the transition rate out of level n_k initiated by the coupling perturbations. More specifically one may think of this perturbation as a timewise modulation of the coupling between the six nn cations caused by the bulk lattice vibrations. We may then use the results of time-dependent perturbation theory[3] to calculate the transition rate

$$1/\tau = (2\pi/\hbar)\,|V'_{if}|^2 \rho_{\text{final}},$$

where ρ_{final} is the density of final states and V'_{if} the perturbation matrix

$$V'_{if} = \langle \chi_{\text{final}}(\vec{q},\vec{Q})\,|\,K\vec{q}\cdot\vec{Q}\,|\,\chi_{\text{initial}}(\vec{q},\vec{Q})\rangle.$$

For the absorption case write (specializing to the case of one mode)

$$\chi_{\text{final}} = \chi_n^{(2)}(q)\chi_i(Q), \quad \chi_{\text{initial}} = \chi_m^{(2)}(q)\chi_j(Q).$$

Then from well-known properties of the harmonic-oscillator functions[3] we have

$$V'_{if} = K\left\{\frac{1}{\alpha_q}\left[\left(\frac{m+1}{2}\right)\delta_{n,m+1} + \left(\frac{m}{2}\right)^{1/2}\delta_{n,m-1}\right]\right.$$
$$\left.\times\,\frac{1}{\alpha_Q}\left[\left(\frac{j+1}{2}\right)^{1/2}\delta_{i,j+1} + \left(\frac{j}{2}\right)^{1/2}\delta_{i,j-1}\right]\right\},$$

where $\alpha_i^2 = m_i\omega_i/\hbar$, subscript i covering both local and bulk oscillators. Conservation of energy requires $\omega_q = \omega_Q$. The two cases, simultaneous absorption ($\delta_{n,m+1}\,\delta_{i,j+1}$) and simultaneous emission ($\delta_{n,m-1}\,\delta_{i,j-1}$) are eliminated by conservation of energy. The assumption that at low temperatures initially all bulk oscillators are in their ground state requires $j = 0$. This eliminates the possibility of the local oscillator absorbing a phonon from the bulk lattice ($\delta_{n,m+1}\,\delta_{i,j-1}$).

Finally we have

$$\frac{1}{\tau_m} \propto \left(\frac{K}{\alpha_q\alpha_Q}\right)^2 \frac{m}{2}\,\frac{j+1}{2}$$

as the lifetime of the mth unrelaxed local vibrational level. The energy width of this level will then be

$$\Delta E_m \sim \hbar/\Delta t_m \propto m. \tag{6}$$

It is hopeless to attempt to calculate an absolute value for ΔE_m since so many factors (i.e., α_i, K, etc.) are "effective" in that they "average" over many complex physical processes. The most one can hope for is a proportionality.

Therefore, we write for the energy width of the nth vibrational level for the kth mode

$$\sigma_{n_k} = \sigma_k^{(0)} + \sigma_k^{(1)} n_k, \tag{7}$$

where $\sigma_k^{(0)}$ is related to the observed half-width of the zero-phonon line and $\sigma_k^{(1)}$ represents a lumping together of all the constants (i.e., α_i, K, $\hbar$, etc.) dropped in the proportionalities leading to Eq. (6). For the assumed Gaussian distributions the observed half-width is equal to $2\sqrt{2}\,|\ln\tfrac{1}{2}|^{1/2}\sigma$. The contribution $\sigma_k^{(0)}$, at low temperatures, is usually due to random strains introduced into the lattice by radiation damage and/or nearby perturbing defects. The size and number of subcrystals and dislocations also affects $\sigma_k^{(0)}$ as it has been found that "proper" heat treatment sharpens the zero-phonon line.

The broadening of phonon structure toward the high-energy portion of the absorption band may alternatively be ascribed to the progressive spread in the frequencies of multiphonon transitions associated with a distribution of lattice frequencies. If a small group of frequencies, in the vicinity of a van Hove singularity in phonon k space, for example, interacts with the F center, the $n > 0$ peaks in fact are smeared to widths proportional to n – precisely the result Eq. (7). A smearing pattern of this form, therefore, is quite general; its presence does not necessarily indicate that only local modes are involved.

Substituting Eqs. (7) and (5) into (4), we have for

low temperatures

$$|\vec{\mu}(E)|^2 \propto \sum_{n_k=0}^{\infty} \prod_{k=1}^{L} B_{k,n_k} e^{-S_k} \sigma^{-1} \exp\left(-\frac{(E-E_0-E_{v1b})^2}{2\sigma^2}\right), \tag{8}$$

where

$$\sigma = \sum_{k=0}^{L} (\sigma_k^{(0)} + \sigma_k^{(1)} n_k).$$

This dipole matrix element may then be used in Eqs. (1) and (2) to predict the shape of the optical absorption $\alpha(E)$ and emission $I^e(E)$ due to F centers in any host material. (We specialize to cubic host materials in Sec. II.) This generalization to any host material is valid because the treatment has not involved specific assumptions regarding the symmetry of the surrounding host lattice. Again, Eq. (8) is not restricted to the optical properties of the F center, but may successfully describe the shape of the optical absorption and emission bands of any impurity of defect center obeying the above-mentioned adiabatic and Condon approximations.

II. VIBRONIC SELECTION RULES FROM SYMMETRY

In this section, selection rules are applied that determine which modes (both local and perfect lattice) may assist an electronic dipole transition when the symmetry of the initial and final electronic state wave functions are known.

It is a general result of group theory that, in order to be nonvanishing, an electric dipole matrix element must be totally symmetric under any operation of the site group. That is, since the site group for F centers in cubic host crystals (alkali halides, alkaline-earth oxides, etc.) is the O_h (cubic) point group, the total matrix element must belong to the Γ_1^+ representation. The representations of the initial (final) system wave functions will be direct products of the representations of the initial (final) electronic wave function and initial (final) vibrational wave function. From previous work[7] it is known that $\phi^{(1)}$ and $\phi^{(2)}$ belong to Γ_1^+ and Γ_{15}^-, respectively. At low temperature the initial vibrational state is the totally symmetric (Γ_1^+) zeroth-order harmonic-oscillator function $\chi_{0_k}^{(1)}$. As the electric dipole operator is vectorlike, it belongs to the Γ_{15}^- representation. These results require that the final-state vibrational wave function $\chi_{n_k}^{(2)}$ belong to the Γ_1^+, Γ_{12}^+, Γ_{15}^+, or the Γ_{25}^+ representative.

First consider the local vibrational modes. A standard vibrational normal-mode analysis[8] of the system of six nn cations harmonically bound by Hookean springs results in eighteen normal modes as follows: three rotational and three translational modes; a nondegenerate Γ_1^+ mode; a doubly degenerate Γ_{12}^+ mode; and triply degenerate Γ_{15}^-, Γ_{25}^-, and Γ_{25}^+ modes. Therefore, of the above final-state vibrational modes only Γ_1^+ (breathing), Γ_{12}^+ (tetragonal), and Γ_{25}^+ (trigonal) modes may be present as local modes with the first excited electronic state.

In order to consider the bulk vibrational modes (lattice phonons), we first reduce the space-group representations for phonons into a sum of defect site-group representations. *A priori* one expects those phonons at high densities of states in the Brillouin zone to be dominant over all those which are allowed by symmetry to be active in phonon-assisted electronic transitions. The reductions, therefore, need be carried out only for special high-density-of-states points on the first Brillouin zone boundary. This reduction has been carried out by Loudon.[9]

Furthermore, in order to make quantitative assignments of vibrational peaks experimentally observed to accompany electronic transitions, it is necessary to know the space-group symmetry assignments at special points in the Brillouin zone. Again, these symmetry assignments have been reported by Loudon for some special high-density-of-states points in the fcc lattice. However, to make even qualitative assignments, somewhat detailed information is required of the dispersion relations $\omega(k)$ and the density of lattice phonon states for the host material. Experimentally, one of the most interesting host crystals in which to study vibrationally assisted electronic transitions associated with the simple F and F' centers is CaO. Other aggregate-defect multielectron trapping centers, such as the R_2 and N centers, show strong phonon peaks in a variety of alkali halides and alkaline-earth oxides.[10] Unfortunately, to date, no complete neutron diffraction results have been reported for CaO so that the details of the dispersion relations remain unknown. Therefore, in order to complete this analysis, some estimate must be made of the frequency of some of these high-density-of-states points near the zone boundary for CaO.

To this end we use the detailed relative density of states and dispersion relations for MgO,[11] a similar cubic material to CaO. Table I summarizes Peckham's results for MgO. Some theoretical considerations[12] on the alkali halides show a similarity in density of phonon states between LiF and NaF, materials similar to MgO and CaO. It is difficult to derive from fundamental considerations a "scale-down factor" for the dispersion relations from one material to another. This is so because the degree of ionicity increases down the alkaline-earth oxide series MgO, CaO, SrO, and because of the paucity of experimental information regarding the interplanor force constants. However, recent infrared optical measurements[13] have placed the Γ point LO and TO modes at 570 ± 7 and 295 ± 0.5 cm^{-1}, respectively, and a most recent tentative neutron diffraction result[14] places

TABLE I. Lattice phonon energies (cm^{-1}) for some special high-density-of-states points in the first Brillouin zone for two alkaline-earth oxides. The results for MgO are taken from Peckham (Ref. 11), while those for CaO (other than TO_Γ, LO_Γ, and TA_X) are only meant to be suggestive.

	MgO[a]				CaO			
	Point in Brillouin zone							
Mode	Γ	X	K	L	Γ	X	K	L
TA	0	305	423	280[b]	0	209[c]	324[a]	192[a,c]
LA	0	430	423	505[b]	0	330	324	387[b]
TO	385	413	479	332	295[d]	317	367	254
LO	702	518	479	674	570[d]	395	367	515

[a]Allowed by symmetry to assist the $\phi^{(1)} \leftrightarrow \phi^{(2)}$ electronic transition in F centers in cubic materials.
[b]Reference 11.
[c]Reference 14.
[d]Reference 13.

TA_X at 209 ± 6 cm^{-1}. These points then may be used in a qualitative manner to scale down the detailed dispersion information for MgO to the CaO case. Table I also lists these results for CaO. Figure 2 superimposes this tentative density of states for CaO with a similarly tentative dispersion relation along the x axis. The symmetry assignments reported by Loudon taken with the reduction coefficients and the above result that only final-state vibrational wave functions belonging to Γ_1^+, Γ_{12}^+, Γ_{15}^+, and Γ_{25}^+ representations then indicate that principally the TA_L and LA_L lattice modes may appear in the vibronic spectra associated with the dipole electronic transition to the first excited state of simple F centers in crystals with the NaCl structure.

III. EXPERIMENTAL

The band-shape functions presented in Sec. I together with the selection rules presented in Sec. II were developed primarily to account for the shape of the optical absorption and emission bands due to F centers in the alkaline-earth oxides. Section III describes the manner by which low-temperature absorption and emission spectra of F centers in CaO and MgO were recorded. We then compare these experimental results with computer-generated plots of Eqs. (1) and (2) employing the vibrational portion of the matrix element expressed in Eq. (8). In these experiments both neutron-irradiated and additively colored samples were used; the former (before irradiation at Oak Ridge National Laboratory) were supplied by W. & C. Spicer Ltd. Winchombe, Glos., England and Semi-Elements Inc., Saxonburg, Pa. and the latter by Hensley, University of Missouri.

A. Procedure

Absorption spectra were taken using a Cary Model 15 recording spectrometer fitted with a small stainless-steel liquid-helium Dewar. Temperature was recorded with a carbon resistor and dc bridge calibrated with a series of fixed-point temperature baths.

Emission spectra were taken with an apparatus specifically designed for this purpose. Samples were mounted in the same Dewar used in the absorption work and were irradiated with monochromatic chopped light. The resulting optical emission focused onto the entrance slit of a Bausch and Lomb 0.5-m grating monochromator blazed for the uv. Of all the emitted radiation only that along an axis perpendicular to the axis of the incident excitation beam and originating from the face of the crystalline sample originally exposed to the excitation light was focused onto the monochromator slit. Other geometries were explored, but this one was found to minimize the self-absorption of the emitted Mössbauer-like zero-phonon line from the F centers in CaO. The exit slit was in turn focused onto a photomultiplier tube. A chopped excitation beam allowed the use of standard phase-sensitive detection techniques. The wavelength sweep rate on this monochromator could be adjusted from 500 to 0.5 Å/min. The dc signal resulting from the lock-in amplifier was fed to a strip chart recorder together with a wavelength indexing signal from the monochromator drive mechanism. The response of the detector system was normalized by comparison to a tungsten filament lamp whose spectral distribution was known over the region of interest.

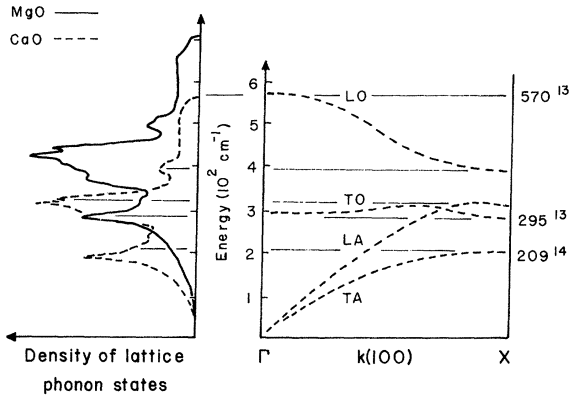

FIG. 2. Tentative dispersion relations and density of lattice phonon states for CaO. This diagram derives from "scaling-down" similar information for MgO (Ref. 11) and fitting to the following three points known for CaO: the two optic modes at the Γ point from ir optical absorption measurements (Ref. 13) and the TA mode at the X point from tentative neutron diffraction results (Ref. 14).

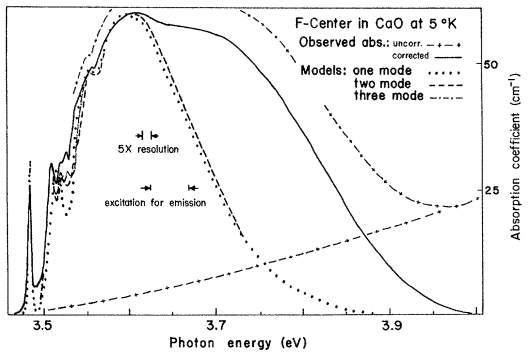

FIG. 3. Absorption due to *F* centers in neutron-irradiated CaO; comparison of low-temperature experimental results with one-, two-, and three-mode absorption shape functions. The uncorrected absorption data are shown together with an assumed base line whereby the "corrected" band is obtained. Most of the model parameters are determined from the observed data (also see text). For the one-mode model ($L=1$) the zero-phonon line is found near 28 114 cm^{-1} and the "average" multiphonon peak spacing is 250 cm^{-1}; thus set $E_0+\frac{1}{2}\hbar\omega_1$ to the former and $\hbar\omega_1$ to the latter. The zero-phonon line half-width is <1 Å; hence set $\sigma_1^{(0)}=12\,cm^{-1}$. The width of the first multiphonon line is <4 Å; hence set $\sigma_1^{(1)}=45$ cm^{-1}. With these parameters we find that an $S_1=4.50$ yields a band whose broad-band peak most closely agrees with that of the (corrected) observed band, where the sum over n_1 was terminated at 15. The best two-mode ($L=2$) parameters are $E_0+\hbar/2(\omega_1+\omega_2)=28\,114$, $\hbar\omega_1=200$, $\hbar\omega_2=300$, $\sigma_1^{(0)}+\sigma_2^{(0)}=12$, $\sigma_1^{(1)}=13$, $\sigma_2^{(1)}=30\,cm^{-1}$, $S_1=1.80$, and $S_2=2.50$. Similarly, the best three-mode ($L=3$) parameters are $E_0+\hbar/2(\omega_1+\omega_2+\omega_3)=28\,114$, $\hbar\omega_1=200$, $\hbar\omega_2=290$, $\hbar\omega_3=360\,cm^{-1}$, $\sigma_1^{(0)}+\sigma_2^{(0)}+\sigma_3^{(0)}=18$, $\sigma_1^{(1)}=13$, $\sigma_2^{(1)}=\sigma_3^{(1)}=15\,cm^{-1}$, $S_1=S_2=1.70$, $S_3=0.90$, and where (for $L=2,3$) n_1, n_2, and n_3 sums were terminated, respectively, at 18, 12, and 10. In those regions where it is not explicity shown, the curve for the three-mode model follows (almost) identically that for the two-mode model.

B. Results

1. *F center in* CaO: *Absorption and Emission*

The *F* center in CaO has been shown to possess an interesting vibronic structure in both absorption and emission.[15,16] Figures 3 and 4 show the recent observed optical absorption and emission, respectively, together with the results of the one-, two-, and three-mode shape functions. In all cases, the theoretical curves have been normalized to the experimental results. The position of the various multiphonon lines and their possible assignment are shown in Table II. The computer analysis was carried out using discrete modes, which may or may not be visualized as local modes. The results of Table II indicate that many of the phonon peaks may be accounted for by considering only the presence of bulk modes. The apparent contradiction here is nonexistent: One may consider, for the purposes of the model, replacing the actual bulk phonon density-of-states distribution (and the symmetry selection rules) by one or two δ functions at ω_1, ω_2, or ω_3 corresponding to high-density-of-states points in the phonon distribution.

For the one-mode shape functions an $\hbar\omega_1$ of 250 cm^{-1} was chosen partially as an average of the first two phonon peaks observed (in absorption and emission) at approximately 200 and 300 cm^{-1} from the zero-phonon line. More support for this choice stems from the temperature-dependence measurements of the broad-band half-width which yields an "effective" electronic ground-state vibrational frequency of 252 ± 6 and 280 ± 20 cm^{-1} for the effective excited-state vibrational frequency[17]; these are from fitting the observed half-width values to the well-known semiclassical expression $\Delta E(T)=\Delta E(0)[\coth(\hbar\bar{\omega}/2kT)]^{1/2}$. The best-fit Huang-Rhys factor was 4.5 for both absorption and emission. This compares favorably to the computed ratio (e^{-S}) between the integrated observed intensities of the zero-phonon transition and the broad bands which yields $S_{em}=4.9$ and $S_{ab}=4.5$.

Fundamental frequencies at 200 and 300 cm^{-1} were chosen for the two-mode models because these were the two lowest peaks in both absorption

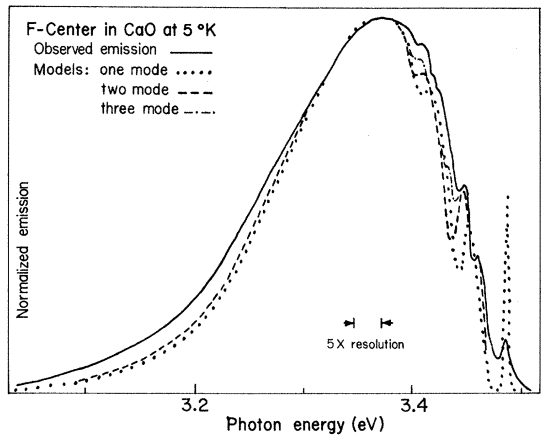

FIG. 4. Low-temperature emission from the *F* center in CaO; comparison of low-temperature experimental results with one-, two-, and three-mode emission shape functions. The best one-mode parameters are identical with those used in the one-mode absorption model (Fig. 3). The best two-mode parameters are again similar to those used in the two-mode absorption model save $\sigma_1^{(1)}=17$, $\sigma_2^{(1)}=38$, $S_1=1.00$, $S_2=3.50$. The best three-mode parameters are again similar to those in Fig. 3 except $\hbar\omega_3=385$, $\sigma_1^{(0)}+\sigma_2^{(0)}+\sigma_3^{(0)}=24$, $\sigma_1^{(1)}=\sigma_2^{(1)}=\sigma_3^{(1)}=17$, $S_1=1.40$, $S_2=1.90$, and $S_3=0.90$. Again, in those regions where it is not shown, the curve for the three-mode model follows identically that for the two-mode model.

TABLE II. Vibronic structure associated with the absorption and emission F bands in CaO (see Figs. 3 and 4) and their tentative assignment.

Absorption			Emission		
Position (cm^{-1})	Separation from zero-phonon line (cm^{-1})	Tentative assignment	Position (cm^{-1})	Separation from zero-phonon line (cm^{-1})	Tentative assignment
$28\,114 \pm 8$	...	...	$28\,114 \pm 12$	...	...
$28\,320 \pm 10$	206	TA_L, Γ_{12}^+	$27\,909 \pm 15$	205	TA_L, Γ_{12}^+
$28\,417 \pm 12$	303	Γ_{25}^+	$27\,812 \pm 15$	302	Γ_{25}^+
$28\,456 \pm 12$	342	LA_L, Γ_1^+	$27\,608 \pm 20$	506	$\Gamma_{12}^+ + \Gamma_{25}^+$
$28\,555 \pm 20$	441	$2\Gamma_{12}^+$	$27\,551 \pm 20$	583	$2\Gamma_{25}^+$
$28\,666 \pm 14$	552	$\Gamma_1^+ + \Gamma_{12}^+$	$27\,481 \pm 20$	633	$3\Gamma_{12}^+$, $\Gamma_{25}^+ + \Gamma_1^+$

and emission. The 205-cm^{-1} peak may be identified with a local mode (Γ_{12}^+) broadened by a TA lattice mode at either the X or L points, or a direct (allowed) coupling to a TA_L mode, or possibly both (near accidental degeneracy).

Further evidence for assigning the strong peak near 200 cm^{-1} in both absorption and emission to a Γ_{12}^+ local mode comes from a moments analysis of Kemp *et al.*[18] where they suggest this mode as possible the dominate noncubic vibrational mode causing a broadening of the Faraday rotation associated with the CaO F center absorption band.

The 302-cm^{-1} line may not be directly associated with any lattice modes because of the symmetry requirements (see Table I), and is therefore most likely a local mode (Γ_{25}^+) broadened by a TO_Γ, TO_L, TA_K, or LA_K lattice mode. In both absorption and emission the $\hbar\omega_2$ mode is seen to couple more strongly to the trapped electron than the $\hbar\omega_1$ mode does, i.e., $S_2 > S_1$. The small peak at 550 cm^{-1} in absorption and at 620 cm^{-1} in the emission shape function is due to the degeneracy of $2\hbar\omega_2$ and $3\hbar\omega_1$. This is observed to split in the emission data yielding the two peaks at 583 and 633 cm^{-1}. The major criticism of the two-mode shape function is the large discrepancy in emission near 400 cm^{-1} and in absorption near 350 cm^{-1}. This is best rectified by introducing a third (weakly coupled) mode at these positions.

Indeed the inclusion of a third weakly coupled ($S_3 = 0.9$) mode does remove most of the above criticism. We interpret the third mode ($\hbar\omega_3$) near 350 cm^{-1} to be the highest-frequency Γ_1^+ local mode broadened by either or both of the optic modes at the K point or a direct coupling to the LA_L lattice mode. The three-mode emission shape function then may quite adequately describe the observed emission band and associated phonon structure. However, the high-energy side of the absorption function deviates markedly from the observed band. Huges[19] has explained this observed partial double-hump character of the absorption band in terms of a Jahn-Teller split excited electronic state caused by the simultaneous (and approximately equal) coupling to both Γ_{12}^+ and Γ_{25}^+ noncubic local modes. A convolution of a double-peaked broad-band shape from the tetragonal mode and a triple peaked band from the trigonal component mode of the Jahn-Teller split electronic excited state together with a smaller ($S_3 = 0.53\, S_2$) coupling to the symmetric Γ_1^+ mode smears out any strong double-peaked character of the main broad band.[20] (Huges's Sec. IV is extremely germane here.)

Our reported Huang-Rhys factors (S_i) are very sensitive parameters. Large-scale computer plots show that even 10% changes in these parameters result in completely different and disagreeable relative phonon strengths with the observed first few phonon-assisted transition peaks in both absorption and emission. The broadening (σ) parameters are somewhat less sensitive, being able to sustain at most 20% alterations before resulting in large disagreement with observations.

These results of the computer calculations also bear out the intuitive notion that the number of modes present does not (necessarily) control the (net) strength of the coupling; that is the total Huang-Rhys factor $S = \sum_i S_i$ should be the same for a one- or many-mode shape function. Inspection of Figs. 3 and 4 shows this to be true. This is evident from Eq. (8) as the model product of exponential terms results in a sum of model Huang-Rhys factors S_k. It is also clear from a configuration-space argument of which Fig. 1 is a single projection ($i = 1$): As $S_i \propto q_i^2$ and $q^2 = \sum_i q_i^2 \propto \sum_i S_i$, then $S \propto \sum_i S_i$.

2. *F center in* MgO: *Absorption and Emission*

As an example of the lifetime broadening model applied to large defect-lattice coupling systems ($S \gg 1$, i.e., classical systems) we include our results for the F center in MgO. A comparison of the observed absorption and emission bands with the results of the one-mode model are shown in Fig. 5. For comparison we also show the re-

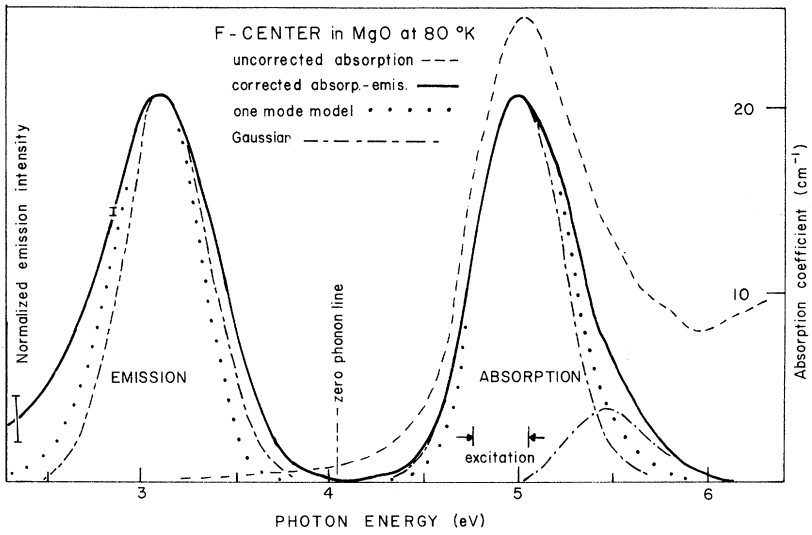

FIG. 5. Absorption and emission bands of *F* center in MgO; comparison of LN temperature experimental results with the one-mode lifetime broadening model and a semiclassical Gaussian approximation. Parameters used in the one-mode model are $E_0+\hbar\omega_1/2=32\,700$ and $\hbar\omega_1=250$ cm^{-1}, $\sigma_1^{(0)}=11$, $\sigma_1^{(1)}=36$ cm^{-1}, $S_1=35$ for emission and $S_1=31$ for absorption. Because there is no phonon structure visible (large Huang-Rhys factor) these results are very insensitive to the σ parameters. This sample was additively colored at 1570 °C at 135-Torr partial pressure Mg. From ESR measurements, $N=1.38\pm0.35\times10^{17}$ cm^{-3}. Application of Smakula's equation to the (corrected) optical absorption data yields $Nf=0.875\times10^{17}$ cm^{-1} yielding an oscillator strength for this system of $f=0.63\pm0.16$. The upper limit on f agrees with previous calculations (Refs. 7 and 23). This somewhat low value of f also suggests a relatively small ratio of F' to F-center concentration as the F' absorption band is thought to nearly coincide with that of the F center in MgO. The low-temperature LHT emission quantum efficiency was generally very low; we estimate $10^{-5}-10^{-6}$.

sults of the semiclassical approximation (valid when $S\gg1$) where the dipole matrix element $\vec{\mu}(E)$ is replaced by a Gaussian distribution of half-width equal to that of our one-mode shape function. We see that the over-all agreement of the one-mode model with the observed bands is better than that of the theoretical Gaussian band; here the appropriate factors of E (absorption) and E^4 (emission) have been included [see Eqs. (1), (2), and (3)]. Actually the Gaussian approximation for the emission band is better than one would expect *a priori* since the E^4 term tends to offset the long low-energy tail. The small discrepancy on the low-energy side is most likely due to a small absorption band centered near 4.3 eV due to the presence (< 10 ppm) of an Fe^{+3} impurity[21] in our samples. On the high-energy side of the absorption band the difference between the observed and model curves suggests a small band centered at 5.43 eV of some 0.16 the integrated intensity of the model band. This may be associated with two small bands at 5.31 and 5.58 eV found by Henderson *et al.*[22] in their Gaussian decomposition of this F-center absorption band. The majority of the poor agreement on the low-energy side of the emission band may be accounted for in terms of an uncertain detector normalization as the error bar indicates and a possible emission from a relatively weak concentration of F' centers that one would expect to the low-energy side of the F-center emission band as is the case for the same defect emission bands in CaO.[17]

For the model calculations, the zero-phonon line was chosen to lie approximately half-way between the absorption peak at 4.94 eV and the observed emission peak at 3.08 eV. The effective ground- and excited-state vibration frequencies are assumed equal and taken from the temperature dependence of the absorption half-width data of Henderson *et al.*[22]

The best-fit absorption model occurred with a Huang-Rhys factor $S^{ab}=31$, somewhat lower than the value of 39 previously reported.[22] All other factors being equivalent in the model calculations, a somewhat higher Huang-Rhys factor ($S^{em}=35$) is required for the emission band because the fourth-order term in energy tends to weigh the emission peak towards higher energy.

Both the absorption and emission bands ostensibly remain the same from 80 °K down to LHT; the bands pictured in Fig. 5 may then be taken to be that of the low-temperature limit. The absorp-

tion band (corrected) half-width was 0.586 eV. The one-mode model half-width is 0.53 eV, somewhat larger than the 0.477 eV reported earlier.[22]

The more nearly Gaussian character of the MgO F-center absorption band, as contrasted with the definite double-humped character of the identical center in CaO, suggests a dominate coupling to a local nondegenerate (Γ_1^+) symmetric mode in the former system. Furthermore, Henderson's measurement of an effective ground-state vibrational frequency $\hbar\omega = 260 \pm 4$ cm^{-1} reflects a possible strong coupling of this local mode to a lattice TA_L mode (see Table I.)

3. R_2 Center in LiF

As an illustrative example of the generality of the ideas developed in Sec. I, we compare the results predicted by the shape function to the low-temperature absorption data for the R_2 center in LiF observed some years ago by Delbecq and Pringsheim.[24] Figure 6 superimposes the one-mode absorption shape function upon the observed data. [The absorption data shown in Fig. 6 are reproduced with the kind permission of one of the authors (Delbecq) of Ref. 24.] The "best-fit" Huang-Rhys factor of $S = 4.3$ is to be compared with that determined from the ratio (e^{-S}) of the observed integrated intensity of the zero-phonon line and the broad band ($S = 3.5$). Neighboring bands and base-line corrections may account for the greater part of this discrepancy. We notice that but one vibrational mode ($\hbar\omega_1$) is required to account for the band shape. *A priori*, it appears that, in spite of the geometric and electronic complexity of the R_2 center as compared to the simplicity of the F center, our one-mode shape function can describe the observed band. However, we wish to express caution here, as the apparent good fit does not reflect an extensive study of this defect center. Nevertheless, our initial results are favorable and may justify further work.

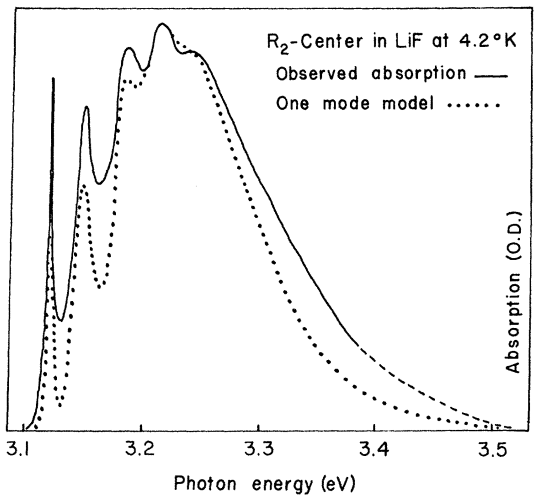

FIG. 6. Comparison of the normalized observed absorption (Ref. 24) and results of the one-mode model ($L = 1$) absorption shape function, Eqs. (1) and (8). Most of the model parameters are determined from the observed data; the zero-phonon line is found near 25 560 cm^{-1} and the multiphonon peak spacing is an average 237 cm^{-1}; hence set $E_0 + \frac{1}{2}\hbar\omega_1$ to the former and $\hbar\omega_1$ to the latter. The reported zero-phonon line half-width is usually a function of spectrometer resolution and sample purity; however, 1 Å agrees with most observers (Refs. 10, 24, 25) yielding $\sigma_1^{(0)} = 11$ cm^{-1}. Similarly by inspection $\sigma_1^{(1)} = 38$ cm^{-1}. The summation over n_1 may be terminated at $n_1 \simeq 2 \times$ (broad-band half-width)$/\hbar\omega_1 \simeq 12$. Then the Huang-Rhys factor S_1 is adjusted so as to make identical the model and observed broad-band peaks; hence $S_1 = 4.3$.

CONCLUSION

We have shown, then, that one may successfully account for the optical emission and absorption band shapes of some defect centers in cubic materials including the relative strengths of many sharp-line (phonon-assisted) vibronic transitions. More specifically our results show that for both CaO and MgO host materials both the transverse and longitudinal acoustic perfect lattice modes near the L band-edge point may couple the F-center electron to the host lattice, and that for the same defect center in CaO both local noncubic (Γ_{12}^+ and Γ_{25}^+) modes couple the trapped electron with the six nn ions to about the same extent with a small additional coupling to the cubic breathing (Γ_1^+) mode. These results are consistent with the findings of other workers.

To complete the alkaline-earth oxide series low-temperature absorption (band peak near 3.1 eV) and emission (band peak near 2.4 eV) spectra were taken for the F center in (neutron-irradiated) SrO. However, as there was no visible phonon structure ($S \simeq 10$) associated with either band, we have not included the complete results here.

ACKNOWLEDGMENTS

One of us (B. D. E.) wishes to thank Professor G. Mahan for helpful discussions about band-edge phonons and Professor K. Park for some experimental assistance. J. Cheng is acknowledged for his construction of a sensitive lock-in amplifier and other technical assistance. Again one of us (B. D. E.) expresses gratitude to Dr. Harvey Schmidt, Jr., for his guidance with the IBM System 360/50 and Calcomp 565 plotter with which the model calculations were preformed.

*Partially based upon a thesis submitted by B. D. Evans for the Ph. D. degree at the University of Oregon, Eugene, Ore. 97403.

†Work supported in part by the Air Force Office of Scientific Research and the Advanced Research Projects Agency.

[1]J. J. Markham, in *Solid State Physics, Suppl.* 8, edited by F. Seitz and D. Turnbull (Academic, New York, 1966).

[2]D. L. Dexter, Solid State Phys. 6, 353 (1958).

[3]L. I. Schiff, *Quantum Mechanics* (McGraw-Hill, New York, 1955).

[4]H. Eyring, J. Walter, and G. E. Kemball, *Quantum Chemistry* (Wiley, New York, 1944).

[5]Reference 2, pp. 364–8.

[6]B. S. Gourary and F. J. Adrian, Solid State Phys. 10, 127 (1960).

[7]J. C. Kemp and V. I. Neeley, Phys. Rev. 132, 215 (1963).

[8]G. Herzberg, *Molecular Spectra and Molecular Structure, II. Infrared and Raman Spectra of Polyatomic Molecules* (Van Nostrand, New York, 1945).

[9]R. Loudon, Proc. Phys. Soc. (London) 84, 379 (1964).

[10]D. B. Fitchen, R. H. Silsbee, T. A. Fulton, and E. L. Wolf, Phys. Rev. Letters 11, 275 (1963).

[11]G. Peckman, Proc. Phys. Soc. (London) 90, 657 (1967).

[12]A. M. Karo, J. Chem. Phys. 31, 1489 (1959).

[13]J. L. Jacobson and E. R. Nixon, J. Phys. Chem. Solids 29, 967 (1968).

[14]J. L. Warren (private communication).

[15]B. D. Evans, J. C. Cheng, and J. C. Kemp, Phys. Letters 27A, 506 (1968).

[16]B. Henderson, S. E. Stokowski, and T. C. Ensign, Phys. Rev. 183, 826 (1969).

[17]B. D. Evans, thesis, University of Oregon, Eugene, Ore., 1969 (unpublished).

[18]J. C. Kemp, W. M. Ziniker, J. A. Glaze, and J. C. Cheng, Phys. Rev. 171, 1024 (1968).

[19]A. E. Huges (unpublished) .

[20]H. C. Longuet-Higgins, U. Öpik, M. H. L. Pryce, and R. A. Sack, Proc. Roy. Soc. (London) A244, 1 (1958).

[21]R. W. Soshea, A. J. Dekker, and J. P. Sturty, J. Phys. Chem. Solids 5, 23 (1958).

[22]B. Henderson, R. D. King, and A. M. Stoneham, J. Phys. C. 1, 586 (1968).

[23]B. Henderson and R. D. King, Phil. Mag. 13, 1149 (1966).

[24]C. J. Delbecq and P. Pringsheim, J. Chem. Phys. 21, 794 (1953), Fig. 13, curve (a).

[25]C. B. Pierce, Phys. Rev. 135, A83 (1964).

PHYSICAL REVIEW B VOLUME 2, NUMBER 10 15 NOVEMBER 1970

Temperature Dependence of *F*-Center Production and Aggregation in NaCl†

E. Sonder
Solid State Division, Oak Ridge National Laboratory, Oak Ridge, Tennessee 37830
(Received 2 June 1970)

The temperature dependence of the vacancy production rate and of the *F*-aggregate-center equilibrium ratio has been measured for electron-irradiated NaCl. The onset of the dose-rate dependence has also been observed. Temperatures obtained from these measurements are compared with the thermal annealing temperature of self-trapped holes and with the temperature at which *F*-aggregate centers form spontaneously in the dark. The maximum vacancy production efficiency occurs near 210 °K; the dose-rate dependence can be observed above 175 °K. These temperatures are significantly below 260 °K at which aggregation occurs. Thus different processes appear to be rate controlling for radiation-defect production on one hand and aggregation on the other. The results support the suggestion that electron-hole recombination at non-defect-producing sites limits defect production at temperatures at which holes are mobile. They also support the idea that aggregate-center formation in the presence or absence of irradiation is determined by motion of F^+ centers.

INTRODUCTION

When KCl is irradiated in the vicinity of room temperature, both the rate of defect production and the *F*-center–*F*-aggregate-center equilibrium depend upon trace impurities, [1,2] irradiation temperature, [3,4] and dose rate. [5,6] It is tempting to try to find a common explanation for the room-temperature defect-production behavior and *F*-center aggregation. The suggestion has been made that mobile negative-ion vacancies (F^+ centers[7]) are involved in defect annealing during irradiation[4]; it also appears probable that these mobile negative-ion vacancies cause *F*-center aggregation. Recent studies[8–12] have shown that in a number of alkali halides, F^+ centers become mobile in an experimentally convenient temperature range, between 200 and 300 °K. Thus the study of the temperature dependence of *F*-center production *and* of *F*-center aggregation appears a very attractive method of testing the thesis that both the net *F*-center production rate and the aggregation are determined by F^+-center mobility.

Several experiments have been performed, mainly with KCl. Comins and Wedepohl[13] have reported that the production rate for *F* centers increases with